Granular flows down inclined channels with a strain-rate dependent friction coefficient. Part I: Non-cohesive materials

Alain de Ryck, Renaud Ansart, John A. Dodds

Granular flows down inclined channels with a strain-rate dependent friction coefficient. Part I: Non-cohesive materials

Alain de Ryck · Renaud Ansart · John A. Dodds

Abstract The flow of a granular material down an incline of finite width with a strain-rate dependent coefficient of friction and a conical yield criterion is semi-analytically obtained using a characteristic method for flows on a deep layer of grains. This analysis leads to a flow field with three distinct zones: a Bagnold-flow zone below the free surface, a dead-zone and a matching zone between the two, linked to slippage at the wall. A good agreement between the computed flow field and experimental data is obtained.

Keywords Granular materials · Surface flows

1 Introduction

The description of dense granular flows is a subject of importance in process engineering and geophysics, including when there is no fluid-particles interactions [7]. Some progress has been made using the lubrication approximation and a Mohr–Coulomb failure criterion [10] or a viscoplastic constitutive equation [1] for the description of non-steady gravitational flows of a finite mass of bulk solids [11]. For a full three-dimensional description, Jop et al. [6] have recently proposed the rheology obtained by introducing a strain rate law in the constant friction model proposed by Jenike [5], leading to:

$$\sigma_{ij} = -P\delta_{ij} + \mu(I)P\frac{\dot{\gamma}_{ij}}{|\dot{\gamma}|}, \tag{1}$$

A. de Ryck (✉) · R. Ansart · J. A. Dodds
École des Mines d'Albi, UMR CNRS 2392,
Route de Teillet, 81000 Albi, France
e-mail: deryck@enstimac.fr

where the apparent coefficient of friction μ depends on an inertial number [3,9]:

$$I = \frac{|\dot{\gamma}|d}{\sqrt{P/\rho}}, \tag{2}$$

which compares the collisional stress with the mean pressure $P = \sigma_{ii}/3$, where σ is the stress tensor. d is the diameter of the particles, ρ the bulk density, $\dot{\gamma}$ is the strain rate tensor and $|\dot{\gamma}| = \sqrt{\dot{\gamma}_{ij}\dot{\gamma}_{ij}/2}$ its second invariant.

This model supposes that the stress and stain rate tensors are co-axial, and a conical yield criterion since we have:

$$|\sigma_{ij} + P\delta_{ij}| = \mu(I)P. \tag{3}$$

It also supposes the conservation of the volume since $\dot{\gamma}_{ii} = 0$, which may restrict its application to shear at the so-called critical state.

With a coefficient of friction dependent on the strain rate, the model is able to predict the flow field since equilibrium or Navier–Stokes equations give a value for the coefficient of friction and therefore to the strain rate. This is not the case of the constant friction model. Nevertheless, some calculations have been performed in this case and Jenike [5], then Cleaver and Nedderman [2], proposed a solution in the case of a radial stress field. In that case, the flow field is obtained within a constant, which is determined using a Bernouilli-like heuristic argument [8].

We propose here a semi-analytical modeling of a straight cylindrical flow identical to the one studied by Partial Differential Integration by Jop et al., based on the characteristic method as in Refs. [5] and [8]. In Sect. 3, we study and comment the Jenike-constant friction solution and in Sect. 4, the general solution is presented for flows on a static layer of grains.

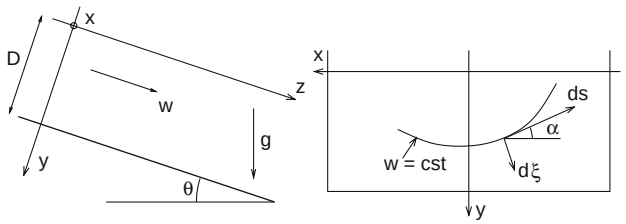

Fig. 1 Sketch of the axis on the incline

2 Mathematical formulation

Let us consider a layer of particles of thickness D flowing stationary on a chute of width $2a$ and inclined by an angle θ from horizontal, as shown in Fig. 1. For a steady-state flow, in the frame sketched on it (x cross co-ordinate, y depth co-ordinate downwards and z along the incline downwards; the origin of the co-ordinates are at the free surface of the granular layer, midway from the walls), the velocities $w(x, y)$ are along the z direction and do not depend on z. Therefore the streamlines are straight lines of constant velocity, there is no convective term in the Navier–Stokes equations which reduce to:

$$\frac{\partial P}{\partial x} = 0, \tag{4}$$

$$\frac{\partial P}{\partial y} - \rho g \cos\theta = 0, \tag{5}$$

$$\frac{\partial}{\partial x}\left(\mu P \frac{\partial w}{\partial x}/|\dot{\gamma}|\right) + \frac{\partial}{\partial y}(\mu P \frac{\partial w}{\partial y}/|\dot{\gamma}|) + \rho g \sin\theta = 0. \tag{6}$$

From the first two equations, we obtain that the pressure is hydrostatic:

$$P = \rho g \cos\theta y. \tag{7}$$

To solve the equilibrium equation along z, it is convenient to define an angle α, such as:

$$\sin\alpha = -\frac{\frac{\partial w}{\partial x}}{|\dot{\gamma}|} \quad \text{and} \quad \cos\alpha = -\frac{\frac{\partial w}{\partial y}}{|\dot{\gamma}|}. \tag{8}$$

α is the local angle that the iso-velocity curve does with respect to the x-axis. By symmetry, for $x = 0$, we have $\frac{\partial w}{\partial x} = 0$, i.e., $\alpha = 0$.

In the following sections, this system will be integrated with a non-slip condition at the wall, first in the case of a constant coefficient of friction (Sect. 3), then in the more general case (Sect. 4).

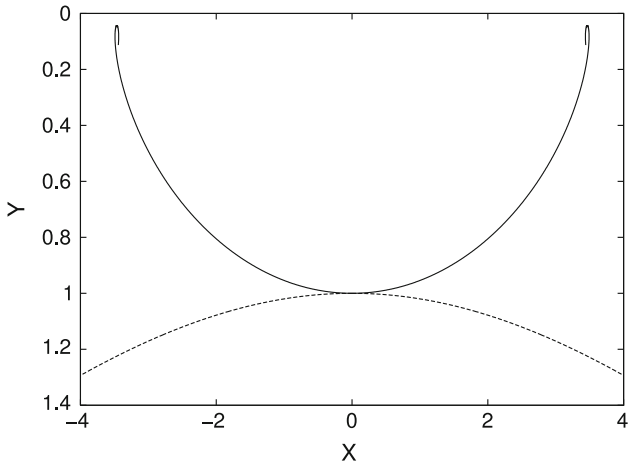

Fig. 2 Characteristics for a constant coefficient of friction and a ratio $R = \tan\theta/\mu = 0.96$ (*dashed line*) and 1.09 (*continuous line*)

3 Constant friction

With the hypothesis of constant friction, Eq. 6 reduces to:

$$y\left(\cos\alpha\frac{\partial\alpha}{\partial x} - \sin\alpha\frac{\partial\alpha}{\partial y}\right) + \cos\alpha - \frac{\tan\theta}{\mu} = 0, \tag{9}$$

which can be integrated as an ordinary differential equation along a s-parametric curve:

$$\frac{dx}{ds} = \cos\alpha y \quad \text{and} \quad \frac{dy}{ds} = -\sin\alpha y. \tag{10}$$

On this curve (which is an iso-velocity since ∇w is normal to it), we have:

$$\frac{d\alpha}{ds} = R - \cos\alpha, \tag{11}$$

where $R = \frac{\tan\theta}{\mu}$. Such a curve can be integrated from the point $(0, h)$ for which we have $\alpha = 0$, or from the point $(0, 1)$ if the lengths x and y are scaled by h (we define $X = x/h$ and $Y = y/h$).

The integration of the system (Eqs. 10, 11) leads to the following parametric equations for the iso-velocity curve:

$$X = \frac{s + \frac{R}{k}\sin(ks)}{1+R}, \tag{12}$$

$$Y = \frac{R + \cos(ks)}{1+R}, \tag{13}$$

where $k = \sqrt{R^2 - 1}$. The detail of this derivation is presented in the Appendix A.

If the slope of the incline is less than μ, then k is a pure imaginary number and the iso-velocity is curved downwards (see Fig. 2, dashed line). Then the curve collides the wall, leading to the conclusion that $w = 0$ everywhere.

If the slope of the incline is greater than μ, then the iso-velocity is a cycloid (see Fig. 2, continuous line). It must

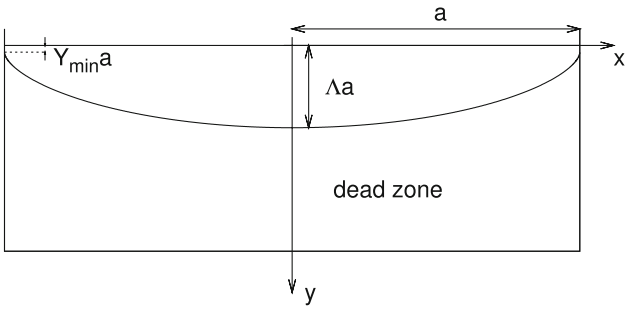

Fig. 3 Deadzone for $R = \frac{\tan\theta}{\mu} = 1.09$ and a granular bed of depth greater than λ times the width

be noted that the curve does not attain the surface of the powder and therefore there is no steady-state solution if the iso-velocity curve does not touch the lateral walls before $\alpha = \pi/2$. As a conclusion, this constant friction model can only define the dead-zone, where the velocity field is null. Its shape may be characterized by the depth of the characteristic tangentially touching the lateral walls. This depth, scaled by the half-width of the channel writes $\Lambda = \frac{h}{X|_{\alpha=\pi/2}}$, leading to:

$$\Lambda = \frac{1+R}{1+\frac{1}{k}\arccos(-1/R)}. \tag{14}$$

If the depth D of the granular layer is higher than Λa, the minimal dead-zone is obtained like in Fig. 3. We may notice that the walls are not entirely included in the dead-zone. The segments between the free surface ($y=0$) and $y = a(1-1/R)$ are above the deadzone.

If the depth of the layer is lower than Λa, there is no solution if the coefficient of friction at the bottom plate is not equal to the slope of the incline.

In this modeling, the velocity gradient may take any value. To fully achieve the resolution of the flow pattern, we need to incorporate a strain-rate dependent coefficient of friction, which is done in Sect. 4.

4 Strain-rate dependent friction coefficient: flows on a layer of grains

4.1 Set of equations

If the coefficient of friction is strain-rate dependent, the equilibrium equation along z (Eq. 6) writes:

$$\mu y\cos\alpha\frac{\partial\alpha}{\partial x} - \mu y\sin\alpha\frac{\partial\alpha}{\partial y} + \sin\alpha\frac{\partial(\mu y)}{\partial x} + \cos\alpha\frac{\partial(\mu y)}{\partial y} = \tan\theta. \tag{15}$$

This equation may be integrated along the curve defined by:

$$\frac{dx}{ds} = \cos\alpha\mu y \quad \text{and} \quad \frac{dy}{ds} = -\sin\alpha\mu y. \tag{16}$$

On this curve, the velocity w is constant since we have $\frac{dw}{ds}=0$. We may define a parameter ξ for the indexation of these iso-velocity curves. We have:

$$\frac{dw}{d\xi} = \frac{\partial w}{\partial x}\frac{dx}{d\xi} + \frac{\partial w}{\partial y}\frac{dy}{d\xi}, \tag{17}$$

then

$$\frac{dw}{d\xi} = -\sin\alpha|\dot\gamma|\frac{dx}{d\xi} - \cos\alpha|\dot\gamma|\frac{dy}{d\xi}. \tag{18}$$

By defining a second family of characteristic (orthogonal to the first one) by:

$$\frac{dx}{d\xi} = \sin\alpha \quad \text{and} \quad \frac{dy}{d\xi} = \cos\alpha, \tag{19}$$

we have on it: $dw/d\xi = -|\dot\gamma|(\xi)$. A particular ξ-line is the y-axis. In this axis, ξ reduces to y-ordinate and we will note $\phi(h)$ the gradient of the velocity profile on it. For a iso-velocity curve starting from the point $(0,h)$, we have: $|\dot\gamma|(\xi) = -\phi(h)$.
Equation 18 reduces to:

$$\frac{d\alpha}{ds} = \tan\theta - \frac{d(\mu y)}{d\xi}. \tag{20}$$

The last term of Eq. 20 may be expanded to gives $\frac{d(\mu y)}{d\xi} = \mu\cos\alpha + (\frac{d\mu}{d|\dot\gamma|}\frac{d|\dot\gamma|}{d\xi} + \frac{d\mu}{dy}\frac{dy}{d\xi})y$. For the iso-velocity curve starting from $(0,h)$, this leads to:

$$\frac{d\alpha}{ds} = \tan\theta - \mu\cos\alpha - \frac{d\mu}{dI}I\left(B(h)\frac{y}{h} - \frac{1}{2}\cos\alpha\right), \tag{21}$$

with $B(h) = h\frac{\phi'(h)}{\phi(h)}$, where the prime denotes the derivation towards h.

For convenience, we may scale the spatial dimensions writing $X = x/\lambda$, $Y = y/\lambda$ and $H = h/\lambda$ with $\lambda = \phi^2(h)d^2/(I_o^2 g\cos\theta)$, where I_o is an arbitrary constant.The inertial number then writes $I = \frac{I_o}{\sqrt{Y}}$. By commodity, since the inertial number I only depends on the reduced co-ordinate Y, $\mu(I)$ will be now written $\mu(Y)$ according to this relation.

The set of equations to solve in order to obtain the shape of an iso-velocity line then writes:

$$\frac{dX}{ds} = \cos\alpha\mu(Y)Y, \tag{22}$$

$$\frac{dY}{ds} = -\sin\alpha\mu(Y)Y, \tag{23}$$

$$\frac{d\alpha}{ds} = \tan\theta - \mu(Y)\cos\alpha + \frac{d\mu}{dY}Y\left(2B(H)\frac{Y}{H} - \cos\alpha\right). \tag{24}$$

The flow zone is obtained by computing the characteristics going to the surface. In order they go upwards, we need $\frac{d\alpha}{ds} > 0$ when $\alpha = 0$. This gives the condition $B < B_{\max}$, with:

$$B_{\max} = \frac{1}{2} + \frac{\tan\theta - \mu(H)}{(\frac{d\mu}{dI} I)|_{I=\frac{I_o}{\sqrt{H}}}}, \tag{25}$$

if $\frac{d\mu}{dI} > 0$ and $B > B_{\max}$ if $\frac{d\mu}{dI} < 0$.

To go further, it is convenient to eliminate the variable α by derivation and reintegration of the Eqs. 22, 23 and 24, in a similar way than the one presented in the Appendix A for the case of a constant coefficient of friction. We obtain:

$$\frac{dX}{ds} = (Y - H)\tan\theta + 2\frac{B}{H}\int_H^Y \hat{Y}^2 \frac{d\mu}{d\hat{Y}} d\hat{Y} + \mu(H)H, \tag{26}$$

together with

$$\left(\frac{dY}{ds}\right)^2 = \mu^2 Y^2 - \left(\frac{dX}{ds}\right)^2. \tag{27}$$

From Eq. 26, we obtain the condition for an iso-velocity line to attain the free surface. We need that $\frac{dX}{ds} = 0$ when $Y = 0$, then that $B = B^*$ with:

$$B^* = H^2 \frac{\tan\theta - \mu(H)}{\int_0^H Y \frac{d\mu}{dI} I dY}. \tag{28}$$

These last equations give a differential equation for the velocity gradient $\phi(H)$ which can be studied more easily defining a function ψ by:

$$\phi(h) = -\frac{I_o\sqrt{g\cos\theta h}}{d} e^{\psi(h)}. \tag{29}$$

Then, the phase diagram for ψ is implicitly given by:

$$\psi = -\frac{1}{2}\log H, \quad \frac{d\psi}{d\log h} = B^* - \frac{1}{2}. \tag{30}$$

Since the end of the resolution is dependent on the exact shape of the ψ-phase diagram, it will be illustrated in the next paragraphs using a particular strain-rate relation.

4.2 Resolution for a given $\mu(I)$ relation

For the next calculations, we use the same $\mu(I)$ relation than the one given in Ref. [6]:

$$\mu(Y) = \mu_s + \frac{(\mu_2 - \mu_s)}{\sqrt{Y} + 1} \quad \text{with} \quad \mu_s = 0.38, \quad \mu_2 = 0.64. \tag{31}$$

With this expression, the phase diagram for ψ is given in Fig. 4. A demonstration *ab absurdo* shows that the unique physical solution is the fixed point. There is no solution for ψ lower than the fixed point due to the fact that there is no

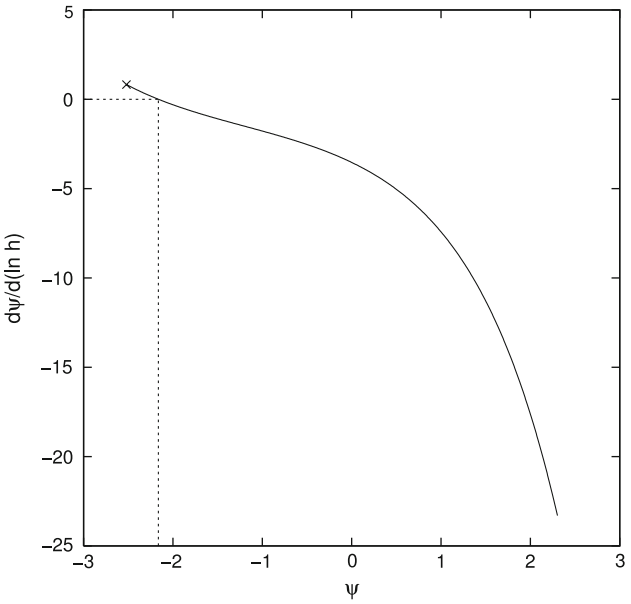

Fig. 4 Phase diagram for ψ for $\theta = 22.6°$ and μ given by Eq. 31. *Left* to the cross, there is no solution ($B^* > B_{\max}$)

characteristics touching the free surface when B is greater than $B_{\max}$. There is no solution for ψ greater than the fixed point since in that case, there is an exponential divergence of the velocity gradient before h attains zero.

Consequently the unique solution, for a given angle θ, is given by the fixed point ($\psi \equiv cst$, $\frac{d\psi}{d\ln h} \equiv 0$). The velocity gradient profile is then parabolic (Bagnold-like):

$$\phi(h) = -\frac{I_o}{d}\sqrt{\frac{g\cos\theta h}{H^*}}, \tag{32}$$

where H^* is the value obtained implicitly from Eq. 28 for $B^* = \frac{1}{2}$.

4.2.1 *Construction of the Bagnold-flow field*

For a given θ, the profile may be integrated using the Eqs. 26 and 27, from the point H^*.

In Fig. 6, the shape of an iso-velocity curve is given for $\theta = 22.6°$ (continuous line). The flowing zone is given by the set of concentric curves above the one touching the free surface at the wall. These iso-velocities curves touch the free surface with a finite slope given by:

$$\left.\frac{dY}{dX}\right|_{Y=0} = -\sqrt{\left(\frac{\mu_2}{\tan\theta}\right)^2 - 1}. \tag{33}$$

From this last equation, we conclude that the depth of this Bagnold-flowing zone h_{Bagnold} goes to 0 when the slope of the incline goes to μ_2 as shown in Fig. 5.

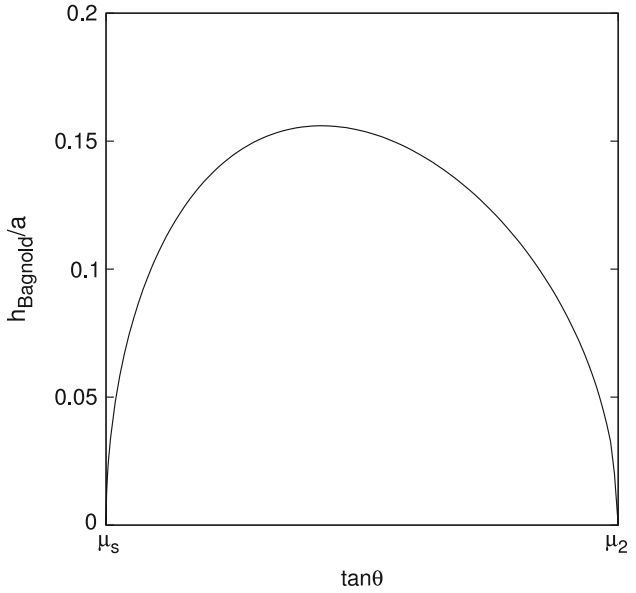

Fig. 5 Depth of the Bagnold-flowing zone h_{Bagnold} scaled by the half width a versus the slope $\tan\theta$

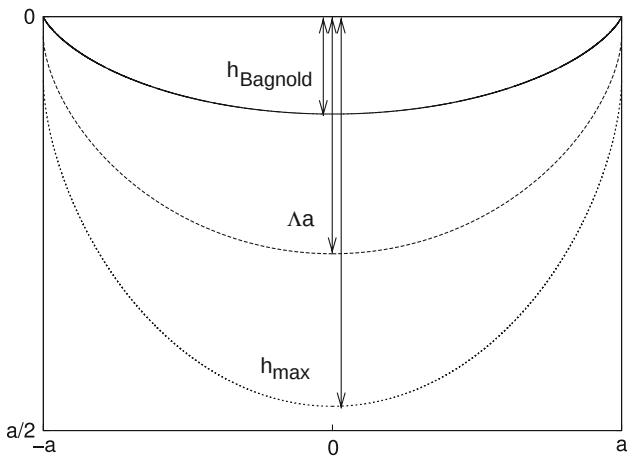

Fig. 6 Flowing and non-flowing zones for $\theta = 22.6°$. Between the free surface and the continuous line, there is a flow with a Bagnold velocity profile. For a constant coefficient of friction, there is no flow below the dashed line. For a strain-rate dependent coefficient of friction, we have a flow zone associated with a slip at the walls between the *dashed* and *dotted lines*. The axis are the same than in Fig. 3

The other point we observe from Eq. 33, and also in Fig. 6, is that there is a region between the Bagnold flowing zone and the deadzone which remains indefinite.

The integration the velocity gradient (Eq. 32) using the no-slip condition at the wall gives the maximal velocity $V_{\max}$ attained at the surface, midway from the walls, and a further integration the flux Q of granular material (per unit width $W = 2a$). The Appendix B gives the analytical expressions, and the quantities Q, $V_{\max}$ and h_{Bagnold}, obtained for the particular relation Eq. 31 with $I_o = 0.28$ are represented in the Figs. 7, 8 and 9 in dashed lines.

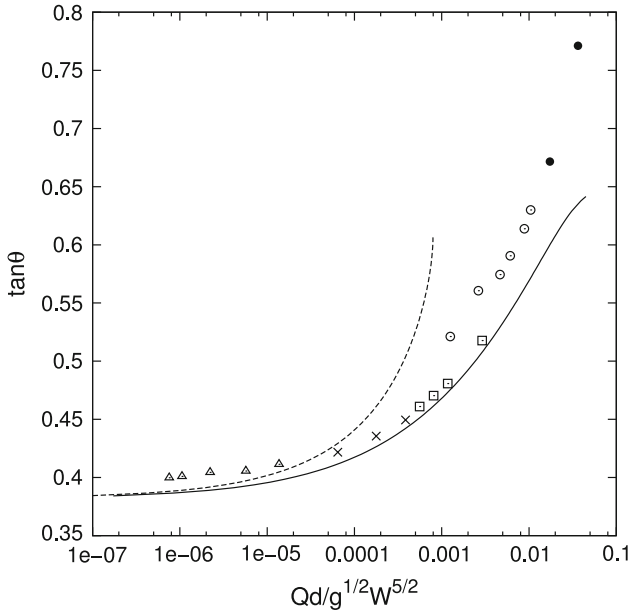

Fig. 7 Slope of the incline versus the scaled flux of granular material. *Dashed line* no-slip at the wall. *Continuous line* with slippage at a rough wall. Points: experimental data for different channel widths from Ref. [6]

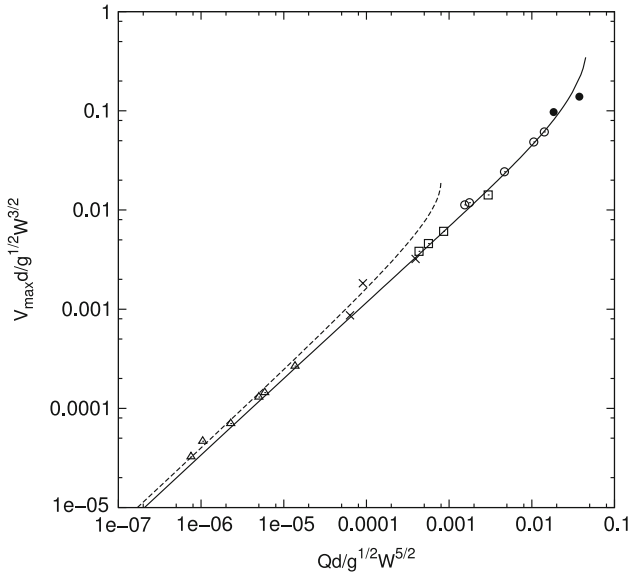

Fig. 8 Scaled maximum velocity versus scaled flux. *Dashed line* no-slip at the wall. *Continuous line* the y-axis is a principal axis of the stress tensor at the wall. Points: experimental data for different channel widths from Ref. [6]

The conclusion is that the hypothesis of no-slip at the wall leads to the good order of magnitude of the velocity field and flux at low incline slopes but unrealistic surface flows when the slope approaches μ_2.

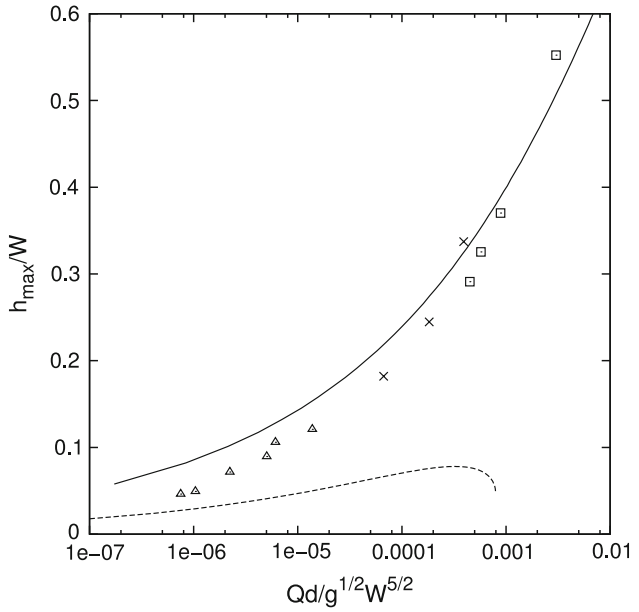

Fig. 9 Scaled maximum depth of the flowing zone versus the flux. *Dashed line* no-slip at the wall ($h_{\text{Bagnold}/W}$). *Continuous line* the y-axis is a principal axis of the stress tensor at the wall. Points: experimental data for different channel widths from Ref. [6]

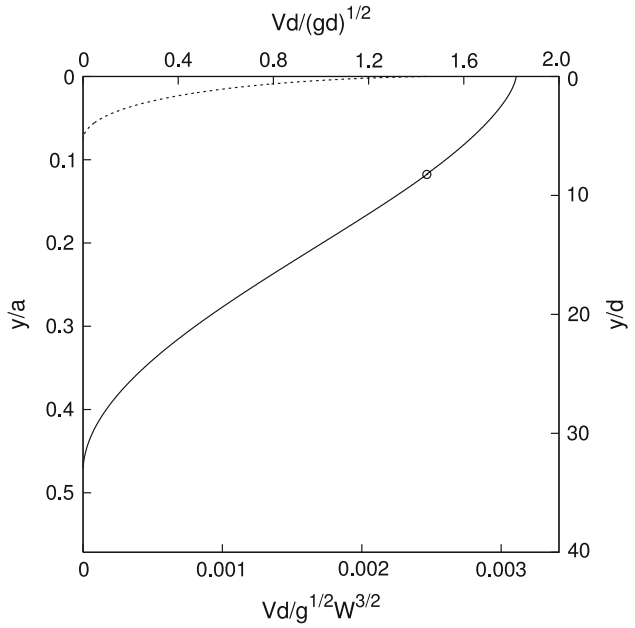

Fig. 10 Scaled velocity profiles at the center ($x = 0$, *continuous line*) and at the walls ($x = \pm a$, *dashed line*). The *circle* gives the beginning of the matching ($w = w(\pm a, 0)$)

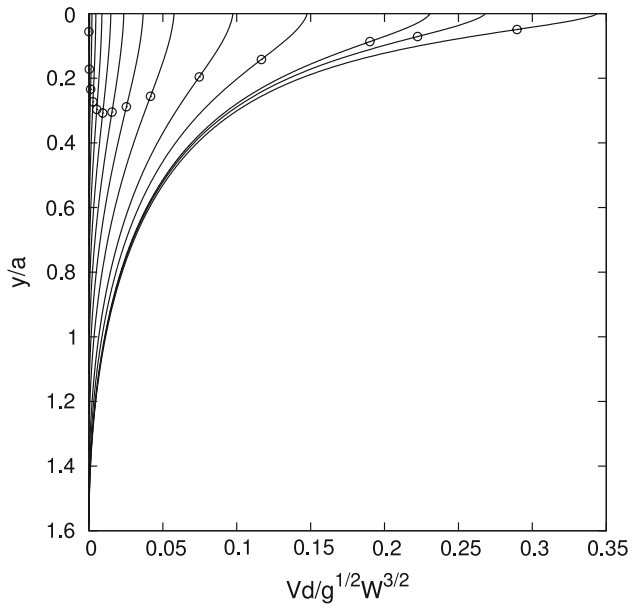

Fig. 11 Scaled velocity profiles for inclination slopes ranging from μ_s to close to μ_2 (respectively, from *left* to *right*). The *circles* give the limit of the Bagnold zone. The three last profiles on the *right* are for slopes equal to 0.991, 0.994 and 0.997 times μ_2

4.2.2 With a matching between the flow and deadzone

If we relax the condition of no-slip at the surface, we may look for a matching between the flowing zone and the deadzone.

In that case, the tangential and normal stresses at the wall (respectively $\tau_w = \mu P \sin\alpha_w$ and $\sigma_w = \mu P$) are related by $\tau_w = \min(\mu_w, \mu)\sigma_w$. P is the local mean pressure, μ_w the wall-powder friction and α_w the value taken by α at the wall. the iso-velocity lines then arrive with an angle $\alpha_w = \arcsin[\min(\frac{\mu_w}{\mu}, 1)]$.

We present such a matching in the case of a rough wall, for which the iso-velocity lines arrive tangentially at the walls. With these hypothesis, we obtain an implicit Ordinary Differential Equation for $\psi(h)$ using the Eqs. 30, 22, 23 and 24, together with the condition $\alpha|_{x\pm a} = \frac{\pi}{2}$, which writes $X|_{\alpha=\frac{\pi}{2}} = \frac{aH}{h}$. By integration of ψ, we obtain the velocity profile for $x = 0$. The Fig. 10 gives the one obtained for $\theta = 22.6°$ (continuous line) and the sliding velocity at the wall (dashed line). The circle in the continuous line gives the beginning of the matching ($w = w(\pm a, 0)$).

The variation of the velocity profile, for slopes ranging from μ_s to μ_2, is given in Fig. 11. We observe in particular that the surface velocity increases more rapidly than the velocities in the bulk when the slope tends to the maximum value μ_2.

The maximal depth of the flow $h_{\max}$, the maximal velocity $V_{\max}$ and flux Q for the different inclination slopes are reported in Figs. 9, 8 and 7 using continuous lines. The results obtained are close to the experimental data obtained by Jop et al. [6].

A final remark about this velocity field with slippage at the wall is that the solutions obtained with the rheology given by Eq. 1 are not regular since the depth of the flow $h_{\max}$ is greater than the depth of the flow zone obtained in the

constant friction case Λa, with Λ given by Eq. 14. As it can be observed in Fig. 6, the iso-velocity line obtained when μ tends to μ_s does not correspond to the iso-velocity line obtained for $\mu \equiv \mu_s$.

5 Concluding remarks

A generic method, based on the study of the characteristics, is developed in order to obtain the steady-state parallel velocity field of a granular media, whose friction coefficient depends on the inertial number I and obeys a conical yield criterion. This method is exemplified with a particular $\mu(I)$ relation and leads to a good agreement with the experimental data if slippage is allowed at the wall and emphasizes the non-regularity of the solution for finite coefficient of friction.

It leads to the conclusion that the flow field may be described by a Bagnold zone below the free surface, followed by a matching zone associated with slippage at the lateral walls near the free surface and then a deadzone, in the case of a granular layer deep enough.

In the case of a flow on a rough plate, i.e. the depth D of the granular layer is lower than the depth of the Bagnold-flowing zone h_{Bagnold}, the solution presented in Sect. 4 is no more valid. This occurs for thin layers on a finite range of slope if the width of the channel is finite, as demonstrated by Fig. 5, or if the width of the incline goes to infinity. In this latter case, there is the following solution for the flow field:

$$w(y) = \frac{2I_e\sqrt{g\cos\theta y}}{3d}(D^{3/2} - y^{3/2}), \quad \text{with} \quad \mu(I_e) = \tan\theta. \tag{34}$$

The study of steady-state solutions for thin flows on rough plate of finite size remains to be investigated.

We have extended this work to the case of cohesive powders as described in the companion paper [4]. Another issue is the non-parallel flows but then, the normalized strain rate tensor cannot be reduced to two components. In such a case, two angles and not only one are necessary to describe the flow, leading to a far more complicated mathematical treatment.

Acknowledgments It is a pleasure to thank Olivier Pouliquen for fruitful discussions.

Appendix A: Equations for the iso-velocity lines for the constant friction case

The derivation of Eq. 10-left gives $\frac{d^2x}{ds^2} = R\frac{dy}{ds}$, using the Eq. 10-right and Eq. 11. By reintegration, this leads to:

$$\frac{dx}{ds} = Ry + h(1-R). \tag{35}$$

In the same manner, by derivation of Eq. 10-right, we obtain $\frac{d^2y}{ds^2} = -R\frac{dx}{ds} + y$. Using Eq. 35,this leads to the second-order differential equation for y:

$$\frac{d^2y}{ds^2} = \left(y - \frac{R}{1+R}\right)(1-R^2). \tag{36}$$

Its integration leads to the parametric Eqs. 12 and 13 for Y and X.

Appendix B: Calcul of the flux for the non-slip condition

The integration of Eq. 32 gives the velocity at the centerline as a function of the depth:

$$w(0,h) = \frac{2}{3}\frac{I_o}{d}\sqrt{\frac{g\cos\theta}{H^*}}\left(h_{\text{Bagnold}}^{\frac{3}{2}} - h^{\frac{3}{2}}\right). \tag{37}$$

The maximal velocity $V_{\max}$ is obtained for $h = 0$. The flux Q per unit width $W = 2a$ writes:

$$Q = \frac{1}{W}\int_0^{h_{\text{Bagnold}}} w(0,h)L_\theta W\frac{h}{h_{\text{Bagnold}}}dh, \tag{38}$$

which gives:

$$Q = \frac{1}{7}\frac{I_o}{d}\sqrt{\frac{g\cos\theta}{H^*}}L_\theta\left(h_{\text{Bagnold}}\right)^{5/2}. \tag{39}$$

where L_θ is the curvilinear length of the isovelocity line passing through the point (0,h_{Bagnold}), scaled by W. L_θ is found to range between 1 and 1.025 for inclined slopes between μ_s and μ_2, when μ is given by Eq. 31.

References

1. Balmforth, N.J., Kerswell, R.R.: Granular collapse in two dimensions. J. Fluid Mech. **538**, 399–428 (2005)
2. Cleaver, J.A.S., Nedderman, R.M.: Theoretical prediction of stress and velocity profiles in conical hoppers. Chem. Eng. Sci **48**, 3693–3702 (1993)
3. Da Cruz, F., Emam, S., Prochnow, M., Roux, J.-N., Chevoir, F.: Rheophysics of dense granular materials: discrete simulations of plane shear. Phys. Rev. E **72**, 021309 (2005)
4. de Ryck, A.: Granular flows down inclined channels with a strain-rate dependent friction coefficient. Part II: Cohesive materials. Granular Matter (2007). doi:10.1007/s10035-008-0106-2
5. Jenike, A.W.: A theory of flow of particulate solids in converging and diverging channels based on a conical yield function. Powder Technol. **50**, 229–236 (1987)
6. Jop, P., Forterre, Y., Pouliquen, O.: A constitutive law for dense granular flows. Nature **441**, 727–730 (2006)
7. Midi, G.D.R.: On dense granular flows. Eur. Phys. J. E **14**(4), 341–365 (2004)
8. Nedderman, R.M.: Statics and Kinematics of Granular Materials. Cambridge University Press, Cambridge (1992)

9. Savage, S.B.: The mechanics of rapid granular flows. Adv. Appl. Mech. **24**, 289–366 (1984)
10. Savage, S.B., Hutter, K.: The motion of a finite mass of granular material down a rough incline. J. Fluid Mech. **199**, 177–215 (1989)
11. Staron, L., Hinch, E.J.: The spreading of a granular mass: role ofgrain properties and initial conditions. Granular Matter **9**, 205–217 (2007)